1828

AKADÉMIAI KIADÓ

Pollack Periodica • An International Journal for Engineering and Information Sciences

21 (2026) 2, 20–28

DOI: 10.1556/606.2025.01394

ORIGINAL RESEARCH PAPER

Check for updates

Evaluation of a dual-purpose solar collector using mono-nanofluids: A CFD simulation

Mustafa Moayad Hasan[1,2*] and Krisztián Hriczó[1]

[1] Department of Analysis, Institute of Mathematics, Faculty of Mechanical Engineering and Informatics, University of Miskolc, Miskolc, Hungary

[2] Department of Mechanical Power Techniques, Basra Technological Technical Institute, Southern Technical University, Basra, Iraq

Received: April 19, 2024 • Revised manuscript received: May 15, 2024 • Accepted: May 16, 2025
Published online: October 10, 2025

ABSTRACT

This study analyzes a dual-purpose solar collector using multi-walled carbon nanotube-water and copper oxide-water mono-nanofluids at a 0.5% volume concentration via computational fluid dynamics in ANSYS Fluent. In the first phase, varying air flow rates showed a 25% temperature increase for nanofluids versus 13% for water, with heat gains of 970.168 W for copper oxide-water and 965.939 W for multi-walled carbon nanotube-water, yielding efficiencies of 62.77 and 56.56%. In the second phase, with constant air flow and varying liquid flow rates, both nanofluids exhibited temperature rises of 4–10 °C, exceeding water's by 2–5 °C. Copper oxide-water provided a heat gain of 1591.93 W and 97% efficiency, while multi-walled carbon nanotube-water reached 1563.19 W and 95%. Conventional water gained 1152.06 W with 70% efficiency. Nanofluids, particularly copper oxide–water, can enhance solar system performance.

KEYWORDS

mono nanofluids, renewable energy, dual-purpose solar collector, computational fluid dynamics, thermal performance

1. INTRODUCTION

The harmful impact of traditional energy sources on the environment and their depletion has accelerated the investment in renewable energy resources, specifically solar energy [1, 2]. Flat Plate Solar Collectors (FPSCs) effectively convert incident solar radiation into heat energy and are commonly used for heating air and liquids. Recently, Dual-Purpose Solar Collectors (DPSCs) have garnered attention for their ability to simultaneously heat both air and liquid in a single device, thereby reducing installation areas and costs by 50% [3].

Numerous techniques have been conducted to enhance the heat transfer rate of collectors, including passive, active, and compound techniques [4]. Passive techniques, which do not require external power, aim to enhance the absorber tubes' heat transfer ability [5]. Methods including twisted tape [6], wire coil inserts [7], and vortex generators [8], are used to create turbulence and improve heat transfer. Additionally, researchers have investigated nano-fluids - comprising solid metals, metal oxides, and carbon nanostructures - as a promising alternative for enhancing the efficiency of flat panel solar collectors (FPSCs) and other thermal applications [9, 10].

Nanofluids, as Heat Transfer Liquids (HTLs), significantly affect the performance of FPSCs due to their high thermal conductivity, low density, and excellent optical properties (absorption, transmittance, and scattering) [11, 12]. Numerous studies on nanofluids have been conducted, however, none have definitively identified the best option due to the varying design parameters, nanoparticle sizes, and conditions [13]. To identify the ideal nanofluid for heat transfer in FPSCs, a focus should be placed on experimental, numerical, and theoretical

*Corresponding author.
E-mail: hasan.mustafa.moayad@student.uni-miskolc.hu, mustafa.hasan@stu.edu.iq

AKJournals

studies that test multiple nanofluids under the same conditions. In this context, Verma et al. [14] investigated the impact of various nanofluids on the energy and exergy efficiencies of a FPSC, using concentrations from 0.25 to 2.0%. The results showed that Multi-Walled Carbon NanoTube (MWCNT)/water nanofluid (0.75 vol%) provided the highest energy efficiency increase of 23.47%, followed by graphene/water (16.97%), CuO/water (12.64%), Al_2O_3/water (8.28%), TiO_2/water (5.09%), and SiO_2/water (4.08%) at a flow rate of 1.5 kg min^{-1}. Ekramian et al. [15] found that MWCNT-water nanofluid provided the highest efficiency at 1 wt% and 3 kg min^{-1}, while CuO-water nanofluid was optimal at 3 wt%. Conversely, SiO_2-water nanofluid showed the lowest efficiency. The solid metal and metal oxide nanoparticles have relatively low density, which may reduce sedimentation issues in FPSCs [16]. Devarajan and Munuswamy [17] investigated the performance of FPSC utilizing CuO, Al_2O_3, and ZrO_2 nanofluids as HTL. They found that at a low rate of 2.8 kg min^{-1}, efficiencies were 55% for CuO, 51.3% for Al_2O_3, 47% for ZrO_2, and 38% for water. Alim et al. [18] examined the impact of various metal oxide nanofluids, including CuO, Al_2O_3, SiO_2, and TiO_2, in a numerical study. In their research, they varied the concentrations of nanoparticles between 1 and 4%, and the flow rates ranged from 1 to 4 kg min^{-1}. The results revealed that CuO/water nanofluid was the most effective, enhancing exergy efficiency and the convective heat transfer coefficient by 4.35 and 22%, respectively. However, pumping power increased by 1.6% at 3 wt% nanoparticle concentration and 3 kg min^{-1} flow rate. In a separate study, Tong et al. [19] evaluated six nanofluids, discovering that MWCNT at 0.005 vol% achieved the highest efficiency of 87%, followed by Al_2O_3 and Fe_3O_4 nanofluids at 1.0 vol%, along with CuO nanofluid at both 0.5 vol% and 0.015 vol%. Additionally, MWCNT nanofluid demonstrated greater sensitivity to changes in operating parameters due to its superior thermal conductivity. Ziyadanogullari et al. [20] prepared three different types of nanofluids - Al_2O_3, CuO, and TiO_2 - to assess the thermal performance of FPSC. The results revealed the highest improvements in energy performance for the Al_2O_3/water nanofluid, which were 71, 63, and 61.1% at concentrations of 0.2, 0.4, and 0.8%, respectively, compared to pure water. For the CuO/water nanofluid, the recorded increases were 87.8, 84.6, and 73.1%, while the TiO_2/water nanofluid achieved increases of 52.5, 47.6, and 35.7% for the same concentrations. These performance differences were mainly due to the varying thermal conductivities of the nanoparticles. In the same context, Hajabdollahi et al. [21] investigated the effects of different nanoparticles (Al_2O_3, SiO_2, CuO) on the design and performance of a solar flat plate collector at various volumetric concentrations. They reported that CuO/water nanofluid demonstrates superior thermal efficiency at a lower volume percentage than other nanofluids tested. Moreover, utilizing CuO/water nanofluid results in a 27.88% reduction in annual costs. Additionally, Al_2O_3/water nanofluid is regarded as a superior circulating fluid due to its lower maintenance requirements and reduced weight. Tong et al. [22] evaluated absorber performance using water, Al_2O_3/H_2O, and CuO/H_2O nanofluids at a flow rate of 0.047 kg s^{-1}. Al_2O_3/H_2O at a volume fraction of 0.01% exhibited the highest efficiency at 77.5%, representing a 21.9% improvement over pure H_2O. In contrast, the CuO/H_2O nanofluid achieved a peak efficiency of 73.9%, representing a 16.2% improvement over water. In a different context, Munuswamy et al. [23] conducted tests using $CuO–H_2O$ and Al_2O_3/H_2O nanofluids in two different absorbers: one equipped with fins and the other without. The findings indicated that the thermal efficiency of the unfinned absorber increased by 2.1 and 4.05% when using 0.2 wt% and 0.4 wt% of CuO nanoparticles, respectively. For the finned absorber, the improvements were 3.02 and 5.5% for the same concentrations. In a separate scenario with Al_2O_3 nanoparticles at different weight percentages, the performance of the unfinned tube collector improved by approximately 3.7 and 6.54%, respectively. The finned tube experienced increases of 4.8 and 7.8% compared to water. Overall, the finned absorber demonstrated significantly better efficiency than the unfinned collector, especially when utilizing nanofluids instead of just water. Hawwash et al. [24] evaluated alumina oxide-water and copper oxide-water nanofluids in FPSC. They theoretically examined the impact of nanoparticle volume fraction and type using a Computational Fluid Dynamics (CFD) model, which was validated against experimental data. The study identified an optimal nanoparticle volume fraction of 0.5% for copper oxide nanoparticles, which achieved the highest thermal efficiency in the collector. Furthermore, copper oxide-water nanofluid was more effective than alumina oxide-water nanofluid under identical conditions. Bazdidi-Tehrani et al. [25] conducted a 3-D numerical model of a ribbed absorber using $TiO_2–H_2O$ and $CuO–H_2O$ nanofluids. They found that increasing the volume concentration of nanoparticles moderately improved the solar collector's efficiency, with $CuO–H_2O$ outperforming $TiO_2–H_2O$. The best performance at 89% was achieved with a 2.04% concentration of $CuO–H_2O$.

In the context of the literature survey, it was observed that among all the investigated nanofluids, MWCNT-water and CuO-water are the most commonly utilized fluids in solar collectors. These nanofluids possess beneficial properties that can enhance the overall thermal performance of solar systems. Consequently, this study examines these two nanofluids at a volume concentration of 0.5% compared to water. A CFD simulation using ANSYS Fluent has been developed to numerically assess the impact of these nanofluids on the thermal performance of a DPSC when used as a heat transfer liquid. While nanofluids have been employed in various solar thermal collectors, there appears to be no prior research specifically investigating their use in DPSCs, making the focus of this study novel. The DPSC modeled in the current study is based on [24] the design fabricated by Assari et al. [26], which features seven tightly spaced triangular air ducts and seven water risers. This work aims to investigate the effects of the two nanofluids on the outlet air and liquid temperatures from the DPSC. Additionally, it assesses the impact of varying air flow rates on exit temperatures, heat gains, and overall thermal efficiency. The CFD simulation results are validated by comparing them with experimental data from Assari et al. [26].

2. NUMERICAL MODELING

2.1. Geometric modeling and meshing

The DPSC modeled in the current ANSYS simulation is identical to that designed by Assari et al. [26]. It consists of seven identical circular tubes and seven triangular air ducts; all units are assumed to perform identically; the schematic of the collector is depicted in Fig. 1.

The specific dimensions and characteristics of the collector, as modeled in ANSYS, are thoroughly outlined in Table 1. This table provides detailed measurements, including length, width, height, and any relevant geometric features of the collector, enabling a comprehensive understanding of its design parameters within the simulation environment.

Since the units of the collector are identical and symmetrical, only half of one unit has been geometrically modeled in the ANSYS Design Modeler as it is shown in Fig. 2a. This model ensures that the mesh elements and nodes are reduced, ultimately lowering the computational cost.

The completed geometry has been transferred to the mesh field of ANSYS, where the appropriate meshing was performed. The sectional view of the meshed model is shown in Fig. 2b.

The generated mesh was meticulously scrutinized through a traditional grid independence test. This critical evaluation aims to determine whether increasing the number of mesh elements results in significant fluctuations in the simulation results. It is essential to confirm that the grid size does not affect the accuracy of the solution [27]. The number of mesh elements was methodically increased from 595,182 to a staggering 1,334,844, yet no notable change in temperature was observed beyond 1,308,692 elements. The quality of the mesh remained comfortably within an acceptable range, ensuring the reliability of the results. Before finalizing the meshing process, every face of the geometry was thoughtfully named, encompassing both the input and output sections. This careful labeling was intended to streamline the setting of boundary conditions during the ANSYS Fluent setup stage.

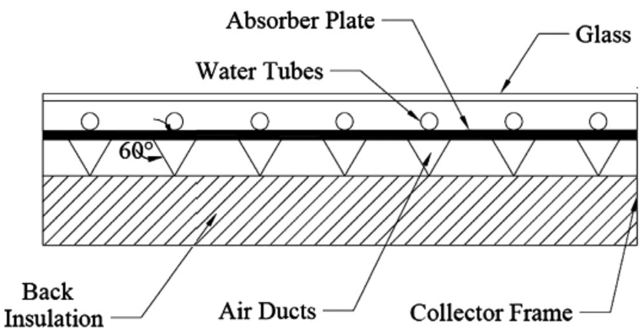

Fig. 1. Schematic of the DPSC used in the current study (*Source*: Authors)

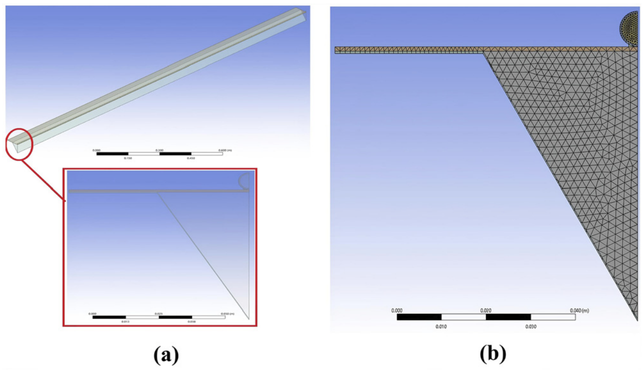

Fig. 2. a) The 3D model of the DPSC, b) Sectional view of the meshed geometry

2.2. Boundary conditions and solution setup

For the current numerical analysis, the following assumptions have been listed below:

1. Steady-state condition;
2. No heat loss through sides and edges;
3. Normal distribution among the risers;
4. The working fluid is incompressible, and its flow is continuous;
5. The absorber and riser materials have constant thermal and physical properties.

In the setup phase, the flow model was defined as laminar, as the Reynolds number fell within the laminar range, with the energy model activated for the entire simulation duration. All materials associated with the collector - comprising both solid and fluid components - were expertly defined and integrated into the simulation framework. Each material was thoughtfully assigned to specific zones within the cell zone conditions. Boundary conditions were applied

Table 1. Detailed specifications of the DPSC

Absorber material	Aluminum sheet, 1.0 mm thickness	Absorber length	1.94 m
Air duct material	Galvanized steel, 0.5 mm thickness	Absorber width	0.95 cm
Cover material	Glazing, 6.0 mm thickness	No. of glazing	1.00
Pipe material	Zinc, 1.0 mm thickness	Pipe diameter	7.00 mm
Air duct shape	Triangle with a 60° angle	Air channel height	6.00 cm

Source: On the basis of [26].

to each of the previously identified named selections in the mesh. At the inlet, a precise mass flow rate and temperature were specified, while the outlet conditions featured atmospheric pressure and temperature. The solar irradiation striking the absorber was represented as heat flux on the upper surface of the absorber. For computational efficiency, a symmetric condition was implemented, as only half of the unit needed to be modeled. This strategic reduction in domain size resulted in a significant decrease in the computational resources required, including memory usage and processing time.

The computational 3D domain is solved using the Semi-Implicit Method for Pressure-Linked Equations (SIMPLE) method and a second-order upwind scheme. The residuals of the simulation are set to be 10^{-6} for energy and 10^{-5} for continuity and momentum. During the solution, a set of critical input parameters was utilized: the solar irradiance was set at 900 W m^{-2}, with the inlet air temperature maintained at 45 °C and the inlet liquid temperature at 40 °C. The air flow rate varied between 0.02 and 0.1 kg s^{-1}, while the liquid flow rate remained consistently fixed at 0.02 kg s^{-1}, ensuring a robust and thorough simulation process.

2.3. Model validation

To rigorously assess the current model and establish its precision and dependability in forecasting outcomes, a thorough validation process has been conducted. Comprehensive data on solar insolation, as well as air and inlet temperatures have been meticulously gathered from the experiments conducted by Assari et al. [26]. Following this, simulations were executed under equivalent conditions to those of the original experiments. The results from the simulations strikingly align with the experimental data, as it is illustrated in Fig. 3. Notably, the absolute average deviation of the outlet temperature from the experimental findings is a mere 0.56%. This striking concordance confirms that the current CFD model of the solar collector has been validated successfully.

2.4. Thermophysical properties of nanofluid

Various researchers [24] have proposed methods for calculating the thermophysical properties of nanofluids. These properties depend on the thermophysical characteristics of the base fluid, the nanoparticles, and their concentration. The equations below present the most widely used correlations for density, specific heat, viscosity, and thermal conductivity of nanofluid:

$$\rho_{nf} = (1-\varphi)\rho_{bf} + \varphi\rho_{np}, \tag{1}$$

$$\left(C_p\right)_{nf} = \frac{(1-\varnothing)\left(\rho C_p\right)_{bf} + \varnothing\left(\rho C_p\right)_p}{\rho_{nf}}, \tag{2}$$

$$\mu_{nf} = (1 + 2.5\varnothing + 6.5)\mu_f, \tag{3}$$

$$K_{nf} = \left[\frac{K_p + 2K_{bf} - 2\varnothing\left(K_{bf} - K_p\right)}{K_p + 2K_{bf} + \varnothing\left(K_{bf} - K_p\right)}\right]K_{bf}, \tag{4}$$

where ρ, C_p, μ, and K represent the density, specific heat capacity, dynamic viscosity, and thermal conductivity, respectively. The subscripts nf, bf, and p denote the nanofluid, base fluid, nanoparticle, respectively. The particle volume fraction refer to by φ.

In the present study, two different types of nanoparticles - CuO and MWCNT - were used to create two distinct nanofluids with water as the base fluid. The volume concentrations of these nanoparticles were set at 0.5%. The thermophysical properties of the base fluid and nanoparticles are summarized in Table 2.

A MATLAB program has been thoughtfully developed to facilitate the calculation of various properties of the nanofluid created. In this code, users can input a range of parameters, including all the properties outlined in Table 2, as well as the volume concentration of the selected nanoparticles. These inputs are then seamlessly substituted into Eqs (1) to (4) to compute the properties of the nanofluid. The calculated properties are carefully stored in a dedicated MATLAB workspace, ensuring they are readily available to serve as inputs for the ANSYS simulation during the definition of materials in the cell zone conditions.

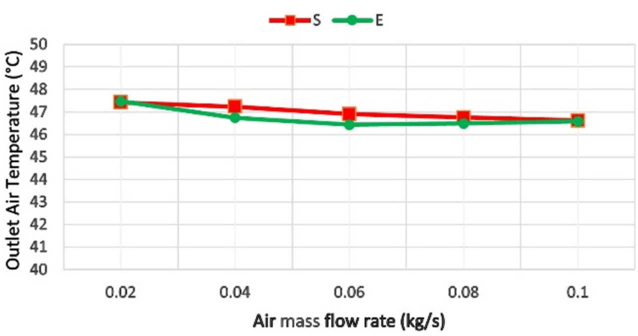

Fig. 3. Validation of the numerical simulation results (S) against experimental data (E)

3. RESULTS AND DISCUSSION

The current work utilized ANSYS Fluent software to investigate the DPSC numerically. The simulation involved two different mono-nanofluids, in addition to water, as heat transfer liquids. The mono-nanofluids used in this study are CuO-water and MWCNT-water, each tested under a volume concentration of 0.5%. As a result, three distinct cases have been created and analyzed using ANSYS simulation. Each

Table 2. The thermo-physical properties of the base fluid and nanoparticles

Physical properties	Water [28]	MWCNT [29]	CuO [24]
ρ (kg m^{-3})	998.2	2100.0	6,000
K (W (m^{-1}. K))	0.613	3,000	33
C_p (J (kg^{-1}. K))	4,182	519	551
μ (mPa·s)	0.001	–	–

case employs unique liquids and the operating parameters specified in subsection 2.2 during the simulation procedure. In this research, two comprehensive case studies of CFD simulations are presented. The first case focused on the impact of varying air flow rates while maintaining all other parameters constant. The second case investigated the effects of changing liquid mass flow rates, while all other parameters remained constant. Both scenarios encompassed a fluid range from 0.02 to 0.1 kg s^{-1} during the simulation period. This approach enabled a thorough analysis of the complex interplay between the air and liquid flows, contributing to a deeper understanding of their dynamic behavior under different operational conditions. It also allowed assessing the impact on outlet air and liquid temperatures as well as efficiency. In total, thirty simulation processes are conducted throughout this study, and the results are discussed in this section.

3.1. The impact of air mass flow rate

The effect of increasing airflow on the outlet air temperature when using different liquids is illustrated in Fig. 4. For all cases, the outlet air temperature exceeds the inlet air temperature. Increasing the air flow rate has a minimal effect on the outlet air temperature when utilizing 0.5% CuO–H_2O and 0.5% MWCNT-H_2O. In contrast, with water, increasing the airflow rate lowers the outlet air temperature from 47.4 to 46.6 °C. For both nanofluids, the increase in outlet air temperature is about 1 °C. However, when using water, the temperature increase is approximately 2.5 °C at an airflow rate of 0.02 kg s^{-1} and 1.6 °C at an airflow rate of 0.1 kg s^{-1}. This difference can be attributed to water's higher specific heat capacity than the tested nanofluids.

In the liquid section of the DPSC, Fig. 5 illustrates the relationship between the outlet liquid temperature and the increasing airflow rate. With an inlet liquid temperature of 40 °C, a significant rise in outlet liquid temperature is observed across all cases. The 0.5% CuO–H_2O and 0.5% MWCNT-H_2O nanofluids achieve the highest outlet temperature, approximately 10 °C higher than the inlet temperature, representing a 25% enhancement. In contrast, water shows only a 13% increase in outlet liquid temperature. This difference may be attributed to the enhanced thermal conductivity of the nanofluids, along with the laminar flow, which increases the time available for the liquids to be heated.

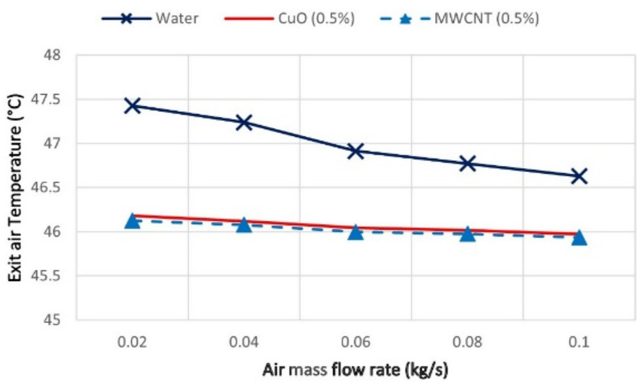

Fig. 4. The effect of airflow rate on the exit air temperature for various HTLs

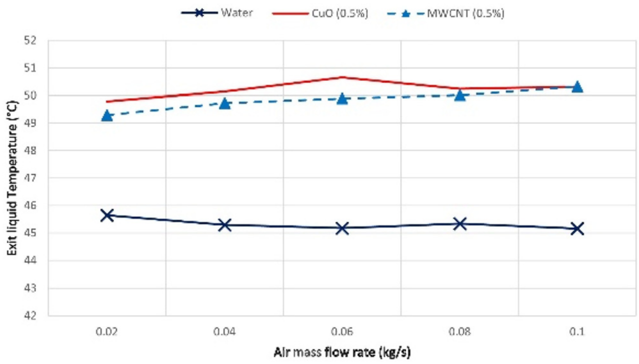

Fig. 5. The effect of airflow rate on the exit liquid temperature for various HTLs

The increase in air mass flow rate results in a temperature drop of approximately 0.5 °C at the liquid outlet when water is used. Furthermore, it is essential to highlight that CuO nanoparticles exhibit superior performance compared to MWCNT in terms of outlet air and liquid temperatures, owing to their greater heat capacity.

The temperature contours across all domains - liquid tube, air duct, and absorber plate - of the DPSC are presented in Fig. 6 corresponding to an air flow rate of 0.06 kg s^{-1}. It shows the temperature contour at a plane located at the DPSC's exit. While the temperature distributions in the liquid sections of both cases presented in Fig. 6a and b are similar, the CuO-water nanofluid demonstrates superior performance on average compared to the MWCNT-water. The lower flow rate, which results in laminar flow, leads to less mixing and weaker heat diffusion throughout the liquid pipe, particularly when using water. In the air section, as depicted in Fig. 6c, the air inside the duct exhibits a uniform temperature distribution compared to Figs. 6a and b, indicating better heat penetration.

The overall performance of the DPSC can be assessed by calculating the total heat gain from the collector's air and liquid components. The total useful heat gain consistently rises for all tested fluids as a higher air flow rate enhances the convective heat transfer, leading to more effective heat absorption. Using CuO at a 0.5% concentration, followed by MWCNT at the same concentration, provides advantages over other liquids circulating in the collector, particularly in terms of total heat gain, as illustrated in Fig. 7. An increase in airflow is correlated with an increase in the total heat gain of the DPSC. The maximum recorded values of heat gain rate are 965.939 W for 0.5% vol MWCNT and 970.168 W for 0.5% vol CuO. In contrast, the minimum recorded values are 801.994 and 843.816 W for the same nanofluids. Both 0.5% vol MWCNT and 0.5% vol CuO showed a maximum enhancement percentage of 58.18 and 58.87%, respectively, compared to using water, which resulted in a lower heat gain.

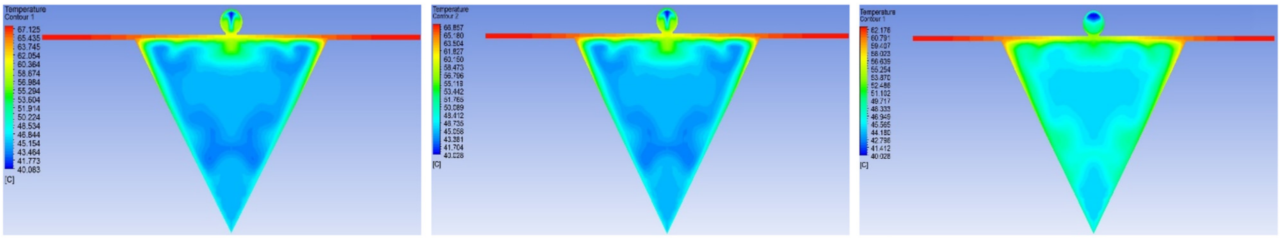

a) b) c)

Fig. 6. Temperature contour of the DPSC under steady-state conditions using different working fluids, a) CuO-Water, b) MWCNT-Water, and c) Water

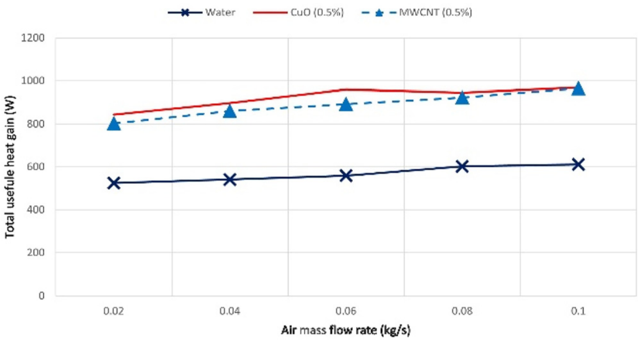

Fig. 7. Variation of useful heat gain with airflow rate for various HTLs

The overall efficiency of the DPSC is significantly affected by the increase in air flow rate, especially when using 0.5% CuO and 0.5% MWCNT nanofluids (see Fig. 8). The average efficiency enhancement is 62.77% for the 0.5% CuO nanofluid and 56.56% for the 0.5% MWCNT nanofluid, compared to water.

3.2. The impact of liquid mass flow rate

After completing the fifteen intricate simulation processes, which focused on varying air flow rates, it became clear that optimal performance was observed at the highest flow rate utilized in the study, specifically 0.1 kg s^{-1}. As vividly depicted in the earlier figures, this optimal flow rate not only fostered maximum efficiency but also elevated the outlet liquid temperature to its peak and harnessed the greatest useful energy. This elevated performance uniquely distinguished it from all other tested rates. Building upon these exciting findings, a series of an additional fifteen simulations explored the fascinating dynamics of the same liquids: water, CuO-water, and MWCNT-water. The liquid flow rate was varied systematically from 0.02 to 0.1 kg s^{-1} while keeping other parameters constant and maintaining the air flow rate at a constant 0.1 kg s^{-1}. Throughout this phase, a thorough analysis was conducted on the effects on both the outlet air and liquid temperatures, the useful heat gain, and overall efficiency, employing the same methodical approach outlined in subsection 2.2 to ensure comprehensive results.

Figure 9 illustrates the relationship between outlet air temperature and various liquid flow rates. As the liquid flow rate increases, the outlet air temperature decreases. Specifically, the temperature reduction is approximately 0.5 °C when water is used, whereas it reaches around 1.5 °C with nanofluids. This reduction can be attributed to the fact that higher flow rate values lead to a shorter heating duration for the liquid as it traverses through the risers. Consequently, this negatively impacts the outlet air temperature, particularly given the already high airflow. This prevents adequate heating of the air due to the high fluid velocity.

The relationship between outlet liquid temperature and liquid mass flow is shown in Fig. 10. As anticipated, the outlet liquid temperature decreases as the liquid mass flow increases. Specifically, when the flow rate of liquid mass increases from 0.02 to 0.1 kg s^{-1}, the outlet water

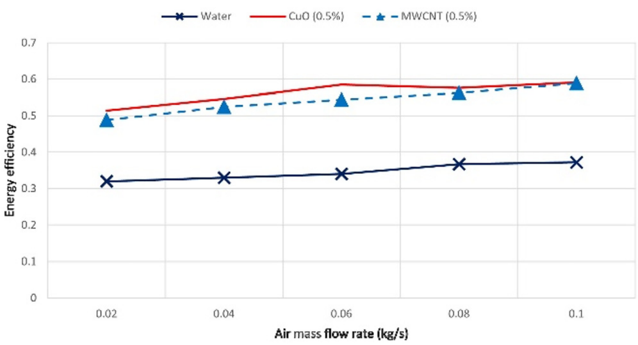

Fig. 8. Variation of energy efficiency (%) with airflow rate for various HTLs

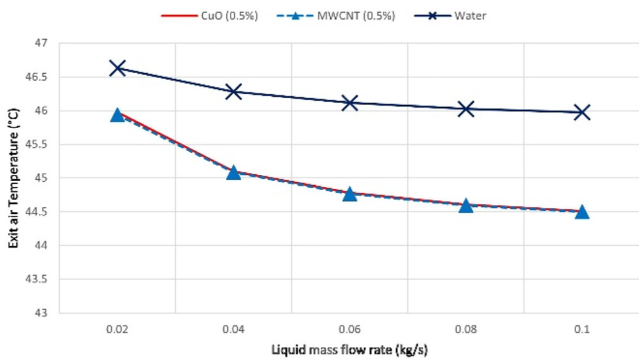

Fig. 9. Variation of exit air temperature with liquid flow rate for various HTLs

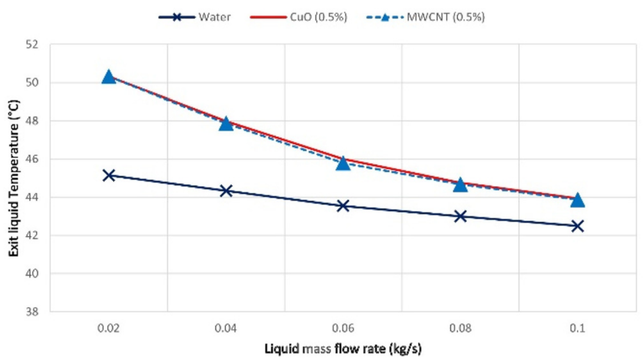

Fig. 10. The effect of liquid flow rate on the exit liquid temperature for various HTLs

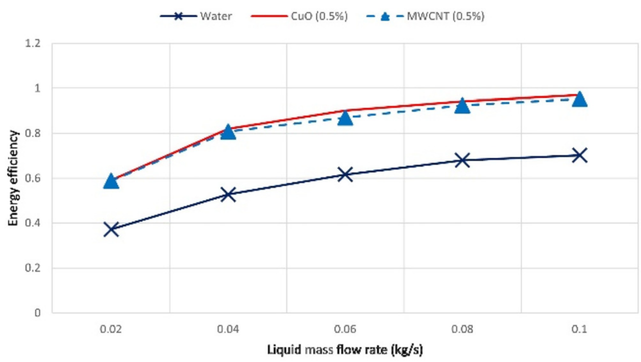

Fig. 12. Impact of liquid flow rate on total energy efficiency (%) for various HTLs

temperature decreases by approximately 2.5 °C. In comparison, the temperature drop for nanofluids over the same flow range is around 6 °C. The increased flow rate shortens the duration of heat exchange between the fluids, resulting in reduced heat transfer and, consequently, a lower outlet temperature. Overall, for all tested liquids, the outlet liquid temperature remains higher than the inlet temperature. For both CuO-water and MWCNT-water nanofluids at a flow rate of 0.02 kg s^{-1}, the outlet temperature increases by about 10 °C, representing a 25% rise over the inlet temperature. In comparison, the temperature increase for water is only 5 °C, corresponding to a 12.5% increase at the same flow rate.

Displaying the temperature contour of the two nanofluids may not provide meaningful insights, as their temperature distributions are identical. Consequently, readers would be unable to differentiate between the contours of the two liquids. Instead, it would be more advantageous to illustrate the useful heat collected from both the air and liquid components of the collector, as well as the associated thermal efficiency. These aspects are depicted in Figs 11 and 12, respectively.

At elevated mass flow rates, the fluid exhibits an increased velocity, resulting in a reduced dwell time within the collector. Consequently, the increment in temperature is minimized. Nevertheless, the increased mass being heated per unit of time leads to an increase in the total energy transferred. Furthermore, this condition also mitigates thermal losses attributable to a lower average fluid temperature, thereby enhancing the efficiency of the collector system.

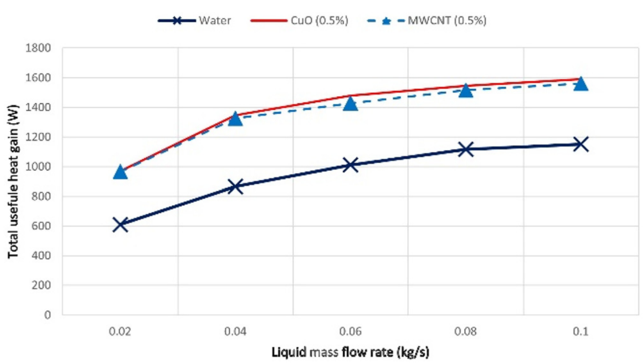

Fig. 11. Impact of liquid flow rate on total useful heat gain for various HTLs

In Fig. 12 the efficiency of the DPSC is improved when using certain liquids and increasing the liquid flow rates. Notably, when water is used as the circulating liquid, the efficiency increases from 37 to 70% as the flow rate rises from 0.02 to 0.1 kg s^{-1}. Additionally, the use of both nanofluids boosts the overall efficiency of the DPSC. At a flow rate of 0.02 kg s^{-1}, both nanofluids demonstrate an enhancement of approximately 59%. At a flow rate of 0.1 kg s^{-1}, the CuO-water nanofluid achieves an efficiency of 97%, while the MWCNT-water nanofluid reaches an efficiency of 95%. This indicates the superiority of CuO over MWCNT.

4. CONCLUSION

In the present study, a comprehensive numerical investigation was conducted using computational fluid dynamics to analyze the performance of DPSC utilizing nano fluids, specifically CuO and MWCNT, at a volume concentration of 0.5%. The thermal performance was compared with that of conventional water.

The investigation was methodically divided into two distinct phases. The initial phase focused on varying air flow rates while maintaining all other parameters constant. The findings indicated that increasing air flow rates significantly enhanced liquid outlet temperatures, with nanofluids exhibiting an improvement of up to 25%, in contrast to a mere 13% for water. The maximum heat gain rates recorded during this phase were 970.168 W for the CuO-water nanofluid, corresponding to an efficiency of 62.77%, and 965.939 W for the MWCNT-water nanofluid, with an efficiency of 56.56%. In comparison, water yielded a heat gain of merely 610.650 W and an efficiency of 37.2%.

In the second phase of the simulation, where the air flow rate was held constant at 0.1 kg s^{-1} and the liquid flow rate was systematically varied from 0.02 to 0.1 kg s^{-1}, notable increase in outlet liquid temperature ranging from 4 to 10 °C were observed for both nanofluids, markedly exceeding the 2–5 °C increase seen with water. The recorded maximum heat gain rates during this phase reached 1591.93 W for the CuO-water nanofluid, 1563.19 W for the MWCNT-water nanofluid, and 1152.06 W for water. Correspondingly, the efficiencies were impressive: 97% for CuO-water, 95% for MWCNT-water, and 70% for water, showcasing the enhanced performance when utilizing nanofluids under optimized conditions.

The research findings underscore the clear advantages of employing nanofluids, specifically CuO-water at a concentration of 0.5%, in enhancing the thermal performance, heat gain, and overall system efficiency of DPSC, thereby suggesting a significant advancement over traditional water-based systems. The superior thermal conductivity and heat capacity of CuO nanofluid were pivotal in achieving these improvements. It was conclusively shown that the DPSC, operating under conditions of an air flow rate of 0.1 kg s^{-1} and a liquid flow rate of 0.1 kg s^{-1}, achieved optimal performance, especially with the application of nanofluids.

Future research could investigate different nanoparticles or hybrid nanofluids at varying concentrations for a more comprehensive analysis. Furthermore, examining the interactions between nanofluids and the collector material is essential, as it may impact long-term performance.

REFERENCES

[1] M. Javidan, M. Asgari, M. Gholinia, M. Nozari, A. Asgari, and D. D. Ganji, “Thermal energy storage inside the chamber with a brick wall using the phase change process of paraffinic materials: A numerical simulation,” *Theor. Appl. Mech. Lett.*, vol. 12, no. 3, 2022, Art no. 100329.

[2] I. Omle, E. Kovács, and B. Bolló, “Applying recent efficient numerical methods for long-term simulations of heat transfer in walls to optimize thermal insulation,” *Results Eng.*, vol. 20, 2023, Art no. 101476.

[3] M. M. Hasan and K. Hriczó, “The optimal approach of various analysis methodologies of a dual-purpose solar collector,” *Pollack Period.*, vol. 20, no. 2, pp. 130–135, 2025.

[4] A. F. Khalaf, A. Basem, H. Q. Hussein, A. K. Jasim, K. A. Hammoodi, A. M. Al-Tajer, I. Omer, and M. A. Flayyih, “Improvement of heat transfer by using porous media, nanofluid, and fins: A review,” *Int. J. Heat Technol.*, vol. 40, no. 2, pp. 497–521, 2022.

[5] S. A. Sakhaei and M. S. Valipour, “Performance enhancement analysis of the flat plate collectors: A comprehensive review,” *Renew. Sustain. Energy Rev.*, vol. 102, pp. 186–204, 2019.

[6] G. Sandhu, K. Siddiqui, and A. Garcia, “Experimental study on the combined effects of inclination angle and insert devices on the performance of a flat-plate solar collector,” *Int. J. Heat Mass Transf*, vol. 71, pp. 251–263, 2014.

[7] A. García, R. Herrero-Martin, J. P. Solano, and J. Pérez-García, “The role of insert devices on enhancing heat transfer in a flat-plate solar water collector,” *Appl. Therm. Eng.*, vol. 132, pp. 479–489, 2018.

[8] F. A. S. da Silva, D. J. Dezan, A. V. Pantaleão, and L. O. Salviano, “Longitudinal vortex generator applied to heat transfer enhancement of a flat plate solar water heater,” *Appl. Therm. Eng.*, vol. 158, 2019, Art no. 113790.

[9] S. P. Tembhare, D. P. Barai, and B. A. Bhanvase, “Performance evaluation of nanofluids in solar thermal and solar photovoltaic systems: A comprehensive review,” *Renew. Sustain. Energy Res.*, vol. 153, 2022, Art no. 111738.

[10] Q. Al-Yasiri, M. Szabó, and M. Arıcı, “Single and hybrid nanofluids to enhance performance of flat plate solar collectors: Application and obstacles,” *Period. Polytech. Mech. Eng.*, vol. 65, no. 1, pp. 86–102, 2021.

[11] R. L. Rashid and A. Hashim, “Maximizing of solar absorption by (TiO_2-water) nanofluid with glass mixture,” *Int. J. Research Eng. Technol.*, vol. 2, no. 1, pp. 87–90, 2014.

[12] R. Saidur, K. Y. Leong, and H. A. Mohammed, “A review on applications and challenges of nanofluids,” *Renew. Sustain. Energy Rev.*, vol. 15, no. 3, pp. 1646–1668, 2011.

[13] Y. Zhang, K. A. Hammoodi, S. M. Sajadi, Z. Li, D. J. Jasim, N. Nasajpour-Esfahani, S. Salahshour, S. A. Eftekhari, and M. K. Khabaz, “Obtaining an accurate prediction model for viscosity of a new nano-lubricant containing multi-walled carbon nanotube-titanium dioxide nanoparticles with oil SAE50,” *Tribol Int.*, vol. 191, 2024, Art no. 109185.

[14] S. K. Verma, A. K. Tiwari, and D. S. Chauhan, “Experimental evaluation of flat plate solar collector using nanofluids,” *Energy Convers Manag*, vol. 134, pp. 103–115, 2017.

[15] E. Ekramian, S. G. Etemad, and M. Haghshenasfard, “Numerical investigations of heat transfer performance of nanofluids in a flat plate solar collector,” *Inter. J. Theor. Appl. Nanotechnol.*, vol. 2, pp. 30–39, 2014.

[16] M. E. Zayed, J. Zhao, Y. Du, A. E. Kabeel, and S. M. Shalaby, “Factors affecting the thermal performance of the flat plate solar collector using nanofluids: A review,” *Solar Energy*, vol. 182, pp. 382–396, 2019.

[17] Y. Devarajan and D. B. Munuswamy, “Analysis on the influence of nanoparticles of alumina, copper oxide, and zirconium oxide on the performance of a flat-plate solar water heater,” *Energy and Fuels*, vol. 30, no. 11, pp. 9908–9913, 2016.

[18] M. A. Alim, Z. Abdin, R. Saidur, A. Hepbasli, M. A. Khairul, and N. A. Rahim, “Analyses of entropy generation and pressure drop for a conventional flat plate solar collector using different types of metal oxide nanofluids,” *Energy Build*, vol. 66, pp. 289–296, 2013.

[19] Y. Tong, X. Chi, W. Kang, and H. Cho, “Comparative investigation of efficiency sensitivity in a flat plate solar collector according to nanofluids,” *Appl. Therm. Eng.*, vol. 174, 2020, Art no. 115346.

[20] N. B. Ziyadanogullari, H. L. Yucel, and C. Yildiz, “Thermal performance enhancement of flat-plate solar collectors by means of three different nanofluids,” *Therm. Sci. Eng. Prog.*, vol. 8, pp. 55–65, 2018.

[21] Z. Hajabdollahi, H. Hajabdollahi, and K. C. Kim, “Multi-objective optimization of solar collector using water-based nanofluids with different types of nanoparticles,” *J. Therm. Anal Calorim.*, vol. 140, pp. 991–1002, 2020.

[22] Y. Tong, H. Lee, W. Kang, and H. Cho, “Energy and exergy comparison of a flat-plate solar collector using water, Al_2O_3 nanofluid, and CuO nanofluid,” *Appl. Therm. Eng.*, vol. 159, 2019, Art no. 113959.

[23] D. B. Munuswamy, Y. Devarajan, M. N. Babu, and S. Ramalingam, “Experimental investigation on lowering the environmental hazards and improving the performance patterns of solar flat plate collectors by employing the internal longitudinal fins and nano

additives," *Environ. Sci. Pollut. Res.*, vol. 27, no. 36, pp. 45390–45404, 2020.

[24] A. A. Hawwash, M. Ahamed, S. A. Nada, A. Radwan, and A. K. Abdel-Rahman, "Thermal analysis of flat plate solar collector using different nanofluids and nanoparticles percentages," *IEEE Access*, vol. 9, pp. 52053–52066, 2021.

[25] F. Bazdidi-Tehrani, A. Khabazipur, and S. I. Vasefi, "Flow and heat transfer analysis of TiO_2/water nanofluid in a ribbed flat-plate solar collector," *Renew. Energy*, vol. 122, pp. 406–418, 2018.

[26] M. R. Assari, H. Basirat Tabrizi, and I. Jafari, "Experimental and theoretical investigation of dual purpose solar collector," *Solar Energy*, vol. 85, no. 3, pp. 601–608, 2011.

[27] I. Omle, A. H. Askar, and E. Kovács, "Optimizing the design of container house walls using argon and recycled plastic materials," *Buildings*, vol. 14, no. 12, 2024, Art no. 3944.

[28] H. Nabi, M. Pourfallah, M. Gholinia, and O. Jahanian, "Increasing heat transfer in flat plate solar collectors using various forms of turbulence-inducing elements and CNTs-CuO hybrid nanofluids," *Case Stud. Therm. Eng.*, vol. 33, 2022, Art no. 101909.

[29] E. Elshazly, A. A. Abdel-Rehim, and I. El-Mahallawi, "4E study of experimental thermal performance enhancement of flat plate solar collectors using MWCNT, Al_2O_3, and hybrid MWCNT/Al_2O_3 nanofluids," *Results Eng.*, vol. 16, 2022, Art no. 100723.